Zero Ion Backflow electron multiplier operating in noble gases

PUBLISHED BY IOP PUBLISHING FOR SISSA MEDIALAB

RECEIVED: *December 8, 2013*
REVISED: *January 14, 2014*
ACCEPTED: *January 14, 2014*
PUBLISHED: *February 14, 2014*

Zero Ion Backflow electron multiplier operating in noble gases

F.D. Amaro,[a,1] **M. Ball,**[b] **J.F.C.A. Veloso**[c] **and J.M.F. Dos Santos**[a]

[a] *GIAN — Physics Department, Coimbra University, Portugal*
[b] *Technical University Munich, Munich, Germany*
[c] *I3N - Physics Depart, Aveiro University, Portugal*

E-mail: famaro@gian.fis.uc.pt

ABSTRACT: We present a novel concept for the suppression of secondary ions in gaseous detectors. The Zero Ion Backflow electron multiplier operates in a noble gas atmosphere and effectively suppresses the ion back flow to the level of primary ionization, totally blocking the secondary ions produced in the multiplier. This detector is composed by a proportional scintillation region, established between two highly transparent meshes, followed by a Gaseous Photomultiplier (GPM). The ionization electrons drift towards the scintillation region, where a proportional electroluminescence signal is produced, without the production of any secondary ionization. A fraction of the emitted VUV scintillation is collected by the photocathode of the GPM and the photoelectron signal is amplified in the GPM through electron avalanche processes. The positive ions of the avalanches developed in the GPM are totally blocked by the mesh that separates the scintillation region and the GPM, resulting in full ion back-flow suppression of secondary ions into the drift/conversion region of the detector. The full suppression capability is independent of the GPM gain. The Zero Ion Backflow electron multiplier is an alternative to readout the ionization signals of Time Projection Chambers in which the accumulation of secondary ions in the sensitive region of the detector has the potential to affect its performance.

KEYWORDS: Time projection Chambers (TPC); Micropattern gaseous detectors (MSGC, GEM, THGEM, RETHGEM, MHSP, MICROPIC, MICROMEGAS, InGrid, etc); Gaseous detectors; Scintillators, scintillation and light emission processes (solid, gas and liquid scintillators)

[1] Corresponding author.

doi:10.1088/1748-0221/9/02/P02004

2014 JINST 9 P02004

Contents

1 Introduction **1**

2 The Zero IBF electron multiplier concept **2**

3 Experimental setup **4**

4 Results **4**

4.1 Extraction field 6

4.2 Optical gain 7

4.3 Total gain and energy resolution 9

5 Conclusions **10**

2014 JINST 9 P02004

1 Introduction

The past years witnessed a series of developments in the field of ion backflow (IBF) reduction in gaseous electron multipliers, motivated by the need to overcome the effects caused by the presence of positive ions in these detectors, particularly in Time Projection Chambers (TPC) and Gaseous Photomultipliers (GPM) equipped with visible sensitive photocathodes [1]–[6].

The introduction of the Gas Electron Multiplier (GEM) [7], with its closed type geometry and the possibility of cascading several elements, lead to a natural improvement on the IBF relatively to the open geometry type multipliers were the IBF is typically 1 [1]. The trapping of the positive ions at the several electrodes of the cascade and the confinement of the electron avalanches to a limited region inside the holes of the GEM results in an effective reduction of the IBF. A carefully optimized choice of parameters in a triple GEM detector operating in a 4 T magnetic field at a gain of 10^3 and drift field of 0.2 kV/cm lead to an IBF value of 0.25% [8]. Nevertheless, despite the significant improvement on the IBF reduction, the values achieved fall short of reaching a desired IBF value of 1/G, being G the detector gain [2].

The trapping of the positive ions at the electrodes of a cascaded multiplier was improved with the Micro Hole and Strip Plate (MHSP) [9, 10], a microstructure that differentiates from the GEM due to the presence of two independent sets of electrodes etched in a strip pattern on one of its faces. The MHSP was operated in the so-called reversed configuration, making use of its thinner strips to additionally trap the positive ions produced in the electron multiplier [4]. This line of research came to a success with the reduction of the IBF to values of 0.03% at a gain of 10^5, allowing for the first time the operation of a GPM equipped with a visible sensitive photocathode in stable, long-term conditions [6, 11].

Another step towards an efficient IBF reduction was the introduction of the Photon Assisted Cascaded Electron Multiplier (PACEM) [5]. The PACEM is a multistage electron multiplier, composed by an MHSP followed by a Gaseous Photomultiplier, operating in a highly scintillating gas,

having an electrostatic ion blocking mesh placed between the two. The secondary scintillation emitted during the electron avalanches that develop in the holes and in the region between the anode and cathode strips of the MHSP is used to propagate the signal on the multiplier through the electrostatic mesh, without the transference of charges between the first element of the cascade, the MHSP, and the following GPM. In addition, the mesh efficiently blocks the ions originated from the GPM and collects most of the ions produced in the electron avalanches taking place around the MHSP anode strips. This configuration operates as an effective opto-coupling signal device. This approach requires the detector to operate in noble gases, CF_4 and/or its mixtures [5, 12] and presents the advantage of the IBF being independent on the electron multiplier gain. The electrostatic separation between the multiplicative stages of the PACEM allows increasing the gain on the GPM, without affecting the overall IBF of the multiplier. The IBF in the PACEM multiplier is, thus, reduced to the ions produced in the first element of the PACEM, the MHSP, and the lowest IBF values obtained in the PACEM, so far, correspond to 2 secondary ions flowing into the conversion/drift region for each primary electron.

Until now these developments have been mostly tailored to the reduction of the IBF on gaseous photomultipliers as the need for IBF suppression on Time Projection Chambers was in most cases fulfilled with the use of gated electrodes inside the detector, at the cost of reduced rate capability [1, 13]. This may not be the case in the future high multiplicity TPCs such as the one foreseen for the ILC, were the build up of the positive ions in the sensitive volume of the detector has the potential to affect its tracking properties due to space charge effects [14–16].

In this work we extend the use of the secondary scintillation emitted by noble gases, already exploited in the PACEM electron multiplier, to the Zero Ion Back Flow electron multiplier concept. The Zero IBF is a multi-stage electron multiplier were the first stage of the cascade is a uniform field, parallel plate region, limited by two highly transparent meshes, operating in the proportional scintillation region regime, i.e. without the occurrence of secondary ionization, in opposition to the case in the PACEM where the electroluminescence is produced in electron avalanches of the MHSP microstructure used as the first stage of the multiplier cascade. Therefore, the only electron avalanches occurring in the Zero IBF multiplier take place on the following GPM stages. Given that there is no charge transfer between the first stage, the proportional region, and the following GPM ones, due to the ion blocking role of the scintillation region mesh, the ion back flow on the electron multiplier is fully suppressed, representing the ultimate stage on ion suppression achievable in gaseous electron multipliers.

The behaviour of the Zero IBF electron multiplier was investigated by recording the pulse height distributions of the output signals as a function the electric fields in the proportional scintillation region and in the region above the CsI photocathode, while irradiating the conversion region with 5.9 keV x-rays.

2 The Zero IBF electron multiplier concept

A schematic of the Zero IBF electron multiplier is presented in figure 1; it is pictured as a Gas Proportional Scintillation Counter (GPSC) [17] readout by a built-in Gaseous Photomultiplier (GPM) [18]. The proportional scintillation region is established between two metallic meshes, G1 and G2. In the actual setup the GPM, placed 2 mm bellow G2, is composed by a CsI photocath-

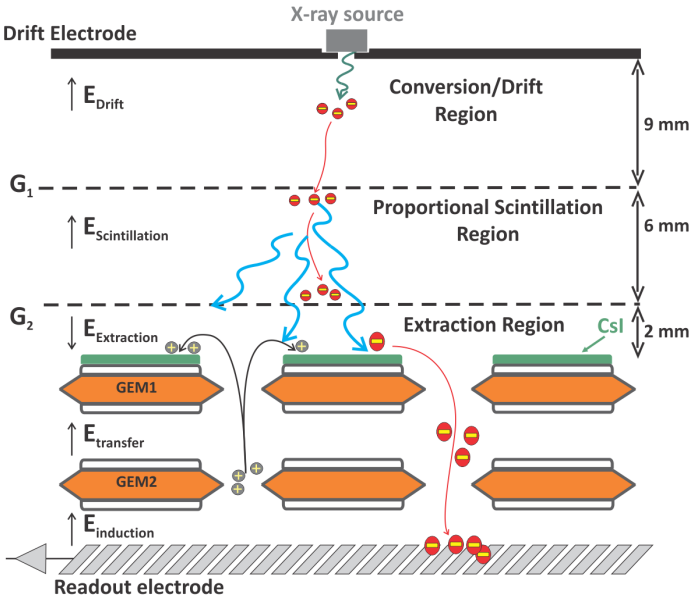

Figure 1. Schematic representation of the Zero IBF electron multiplier. The first stage is setup between the meshes G1 and G2, delimiting a Proportional Scintillation region, which is followed by a built-in Gaseous Photomultiplier, here consisting of a double GEM detector coupled to a CsI photocathode.

ode coupled to a double GEM electron multiplier (D-GEM) but other cascades of gaseous electron multipliers are valid options. The reflective CsI photocathode (2500 Å thick) was deposited on the top electrode of the first GEM of the cascade by vacuum thermal deposition, making it sensitive to UV photons up to 210 nm [18].

The ionizing radiation interacting with the atoms of the gas in the conversion/drift region, between the cathode electrode and G1, produces a primary electron cloud that drifts towards the proportional scintillation region. The electric field in this region is set to a value between the gas thresholds for scintillation and ionization (about $0.8\,\mathrm{kV}\times\mathrm{cm}^{-1}\times\mathrm{bar}^{-1}$ and $4.6\,\mathrm{kV}\times\mathrm{cm}^{-1}\times\mathrm{bar}^{-1}$ for xenon, respectively [19]). Under the influence of this electric field the primary electron cloud drifts through the scintillation region, causing the excitation of a large number of the gas atoms without the production of secondary ionization, followed by the emission of a large amount of VUV photons. Their number is dependent on the electric field value and on the depth of the scintillation region: for an electric field of $4\,\mathrm{kV}\times\mathrm{cm}^{-1}\times\mathrm{bar}^{-1}$ and a 6 mm deep scintillation region around 350 VUV photons are produced per each primary electron [19]. This secondary scintillation is emitted isotropically and a fraction of the VUV photons reaches the CsI photocathode deposited on the top electrode of the first GEM of the GPM cascade, inducing the extraction of photoelectrons. The photoelectrons are focused into the holes of the GEM were they undergo charge avalanche and from where the resulting avalanche electrons are extracted and transferred into the next GEM of the cascade. Another charge avalanche takes place in this element, being the final charge collected at the readout electrode. This concept can be applied to other noble gas filling such as argon [20] or mixtures of argon and/or xenon with other noble gases.

A fraction of the ions resulting from the avalanche mechanisms in the GPM is collected at the several electrodes of the double GEM cascade. Depending on the electric field value between

2014 JINST 9 P02004

mesh G2 and the first GEM top electrode, $E_{EXTRACTION}$, the secondary ions produced in the GPM are prevented of reaching the conversion/drift region of the detector if mesh G2 is at a somewhat higher potential than that of the top electrode of the first GEM. In this case, since no secondary ions are produced on the scintillation region, the only ions present on the conversion/drift region are the ones resulting from the primary ionization.

3 Experimental setup

The Zero IBF detector has been investigated within a stainless steel vessel, evacuated down to 10^{-6} mbar prior to gas filling. The detector was operated in pure xenon (99.99%) at the pressure of 1.3 bars. The gas was purified by circulation through non-evaporable getters, SAES St707, placed in an adjacent volume to the detector and kept at 200°C. The detector is isolated from the purifying system by means of two valves placed at both entrances of the detector. The electrical connections are made of high vacuum compatible MACOR feedthroughs. The electrodes of the detector were independently polarized using CAEN N471A power supplies with current limitation (80 nA).

The GEMs are made from 50 μm thick Kapton® foil with 28 mm^2 active area, covered on both sides with a gold-plated 5 μm copper layer. The Kapton foil is micro-perforated with bi-conical 70/50 μm outer/inner diameter holes, arranged in hexagonal pattern with a pitch of 140 μm.

The conversion/drift region (9 mm wide) was limited by the drift electrode, a 2 mm thick stainless steel plate, and by mesh G1. The drift electrode has a 1 mm aperture that collimates the 5.9 keV x-rays emitted by a ^{55}Fe source placed on top of this electrode. A 0.045 mm thick Cr film was placed between the ^{55}Fe source and the drift electrode, acting as attenuator while filtering the 6.49 keV k_β line.

The scintillation region, limited by the meshes G1 and G2 (80 μm diameter wires, 900 μm spacing), was 6 mm wide. The gap between grid G2 and the CsI photocathode was 2 mm; the same distance was kept between each GEM of the cascade and between the last GEM and the readout electrode.

The final avalanche-charge per event was recorded from the readout electrode with a Canberra 2006 preamplifier (sensitivity set to 47 mV/MeV) followed by a Tennelec TC 243 linear amplifier (8 μs shaping time) and a Nucleus PCA 2 multichannel analyzer. The electronic chain sensitivity was calibrated by injection of a known charge into the preamplifier input.

4 Results

Figure 2 presents a typical pulse height distribution obtained with the Zero IBF electron multiplier when irradiating the conversion/drift region with 5.9 keV x-rays from the ^{55}Fe x-ray source. The electric fields in the conversion/drift region, in the scintillation region and in the extraction region were set to 60 V$\times$cm$^{-1}\times$bar^{-1}, 4.6 kV$\times$cm$^{-1}\times$bar^{-1} and 0.20 kV$\times$cm$^{-1}\times$bar^{-1}, respectively. The voltage difference applied to the first and second GEM of the cascade was 410 V and 490 V, respectively. The transfer and induction fields were set at 1.2 and 1.8 kV$\times$cm$^{-1}\times$bar^{-1}.

The signal corresponding to the electron amplification in the avalanches of the GEM cascade can be obtained using the signals induced by the x-rays in the absence of secondary scintillation in the region between G1 and G2. This can be achieved by setting the electric field between G1

2014 JINST 9 P02004

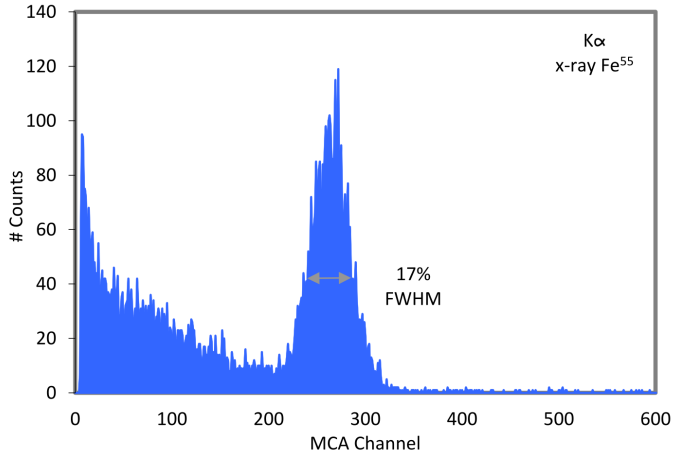

Figure 2. Typical pulse height distribution for 5.9 keV X-ray interactions on the drift region recorded with the Zero IBF electron multiplier, for an electric field in the scintillation region of 4.7 kV×cm^{-1}×bar^{-1}.

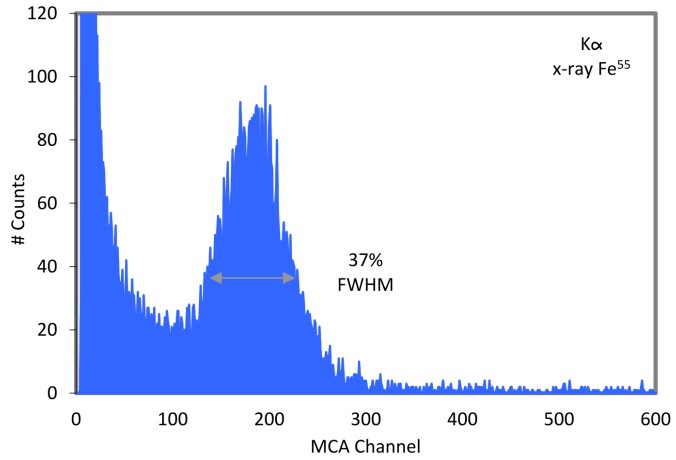

Figure 3. Typical pulse height distribution for 5.9 keV X-ray interactions in the drift region obtained for the double-GEM cascade avalanches only, i.e. without having the production of secondary scintillation in the Zero IBF electron multiplier, for the biasing conditions described in the text.

and G2 to a value bellow the scintillation threshold in the gas and reversing the extraction field (relative to the direction presented in figure 1). Under this configuration the primary electrons are transferred from the conversion/drift region to the proportional scintillation region and finally to the extraction region, without the production of secondary scintillation. The primary electron cloud is then multiplied in the D-GEM cascade. Figure 3 presents a typical pulse height distribution obtained in these conditions, resulting from the direct interactions of the 5.9 keV x-rays in the absorption/drift region. In the present case, the electric fields in the absorption and scintillation regions were set at 60 V×cm^{-1}×bar^{-1}, a value bellow the onset for scintillation in the gas. The extraction field (600 V×cm^{-1}×bar^{-1}) was inverted relatively to the direction presented on figure 1. The voltage differences on the first and second GEM were 440 V and 540 V, respectively. The transfer and induction fields were 1.2 and 1.8 kV×cm^{-1}×bar^{-1}.

2014 JINST 9 P02004

The electric field configuration used for the measurement of the electron amplification in the avalanches of the GEMs in the absence of scintillation in the proportional scintillation region, were the electric fields in the absorption and scintillation regions were set at $60\,V\times cm^{-1}\times bar^{-1}$, does not assures a full electron transfer efficiency through G1. For this electric field configuration, a value of 0.25 was measured for the electron transparency of mesh G1. This value has to be taken into account to obtain the overall gain of the GPM and, then, to estimate the optical gain of the proportional scintillation stage, i.e. the average number of photoelectrons focused into the first GEM holes per primary electron crossing the scintillation region. This value can be obtained through the ratio of the amplitudes of the electron multiplier pulses when operating in both modes, with and without proportional scintillation.

The mesh G1 electron transparency for the above mentioned electric field configuration also explains the high value obtained for the energy resolution of the double GEM cascade (figure 3) that should be close to 25% [21]. If we scale the energy resolution with $Ne^{-1/2}$, being Ne the number of primary electrons reaching the GEM holes, the energy resolution of the double GEM cascade would be a factor of two lower for a mesh G1 electron transparency of 1.

4.1 Extraction field

The extraction of the photoelectrons from the reflective photocathode and their focusing into the holes of the first GEM of the cascade are strongly influenced by the electric field in the extraction region above the CsI photocathode ($E_{EXTRACTION}$ in figure 1). In the absence of a voltage difference between the top electrode of the first GEM and mesh G2 the photo-electron extraction is controlled by the electric field established between the top and bottom electrodes of the first GEM. This field extends itself into the region above the top electrode of the GEM, were the CsI photocathode is deposited, reaching values that assure an efficient photoelectron extraction [18]. On the other hand, the electric field in the extraction region controls the ion backflow crossing this region and a value high enough will be able to suppress this flow, figure 1.

The dependence of the ion backflow and the photoelectron extraction efficiency on $E_{EXTRACTION}$ was evaluated by operating the Zero IBF electron multiplier in current mode: the ^{55}Fe x-ray source was replaced by an HgAr lamp, emitting VUV photons. The VUV photons promoted the photo-electron extraction from the CsI photocathode and the photoelectrons were, subsequently, focused into the GEM holes and multiplied in the double-GEM cascade. The relative photoelectron extraction efficiency was measured from the electron current recorded in the induction plane while the IBF was measured from the ion current recorded in mesh G1.

A negative field in the extraction region (i.e. $E_{EXTRACTION}$ pointing to G2, figure 1) reduces the photoelectron extraction efficiency (figure 4: open circles, right axis) as it overcomes the effect of the electric field established between the top and bottom electrodes of the first GEM of the cascade, reducing the possibility of photoelectron escape from the CsI photocathode. On the other hand, a positive value of $E_{EXTRACTION}$ (i.e. $E_{EXTRACTION}$ pointing to the photocathode, figure 1) is favourable to the photo-electron extraction from the CsI photocathode but not to its focusing into the holes of the GEM, as the photo-electrons tend to be collected in G2. This effect is present in figure 4 were the photoelectron extraction efficiency decreases for values of $E_{EXTRACTION}$ above $0.2\,kV\times cm^{-1}\times bar^{-1}$. This latter effect is slightly compensated above the threshold for excitation in xenon ($\approx 1\,V\times cm^{-1}\times torr^{-1}$) since the photoelectrons traversing the extraction region towards

2014 JINST 9 P02004

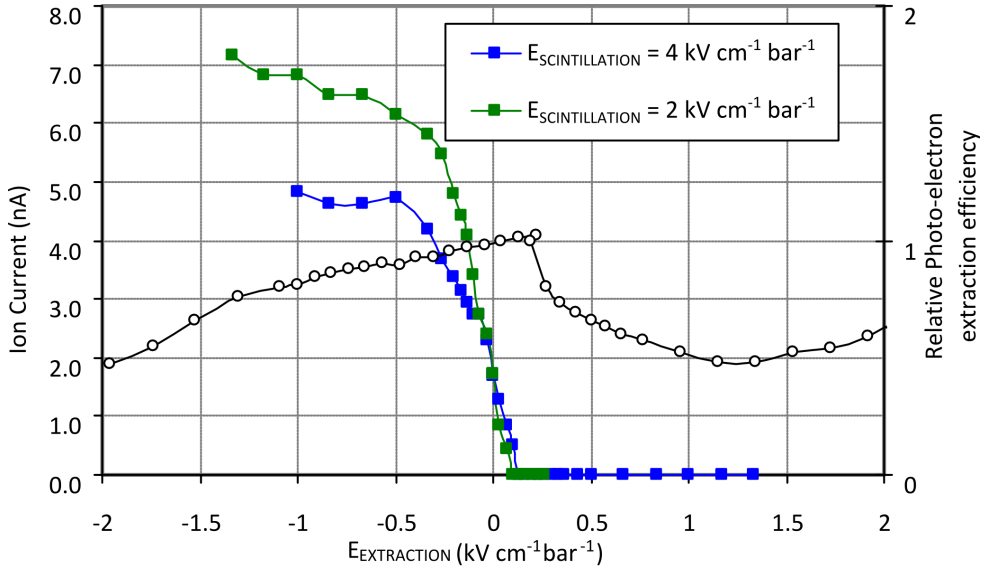

Figure 4. Relative photoelectron extraction efficiency (open circles, right axis) and Ion current reaching the mesh G1 (solid squares green and blue, left axis) as a function of the field in the extraction region, above the photocathode. The relative photo-electron extraction curve was obtained for $\Delta V_{GEM1} = 410$ V.

G2 produce additional secondary scintillation, releasing extra photoelectrons and, thus, contributing to an overall increase of the photoelectron current. The maximum photoelectron extraction and its focusing into the GEM holes is achieved for a small region of $E_{EXTRACTION}$ values, which extends from a null $E_{EXTRACTION}$ to slightly positive values, under $0.2\,kV\times cm^{-1}\times bar^{-1}$.

The ion current that reaches mesh G1 is also presented in figure 4 as a function of $E_{EXTRACTION}$ (solid squares, left axis). During this measurement, to ensure that all the positive ions were collected at mesh G1, the electric field between the drift electrode and mesh G1 was reversed. For negative values of $E_{EXTRACTION}$ (relative to the direction presented in figure 1) the positive ions are transferred from the extraction region to the scintillation region. However, for $E_{EXTRACTION}$ above $0.1\,kV\times cm^{-1}\times bar^{-1}$ the secondary ions produced on the GPM do not have enough energy to cross the extraction region and are trapped on the top electrode of the first GEM of the cascade, being completely prevented from reaching the scintillation region.

Therefore, the Zero Ion Back Flow electron multiplier should preferably be operated with $E_{EXTRACTION}$ between 0.1 and $0.2\,kV\times cm^{-1}\times bar^{-1}$ since this region of operation ensures simultaneously full ion back flow suppression and maximum photo-electron extraction efficiency.

4.2 Optical gain

The optical gain of the Zero IBF detector is defined as the number of photoelectrons extracted from the CsI photocathode and focused into the GEM holes, for each primary electron [5]. In our measurements this figure was obtained from the ratio between the amplitudes of the scintillation peak and the peak obtained without secondary scintillation production, for identical voltages on the GPM, after correcting for the grid electron transparency of G1. The grid G1 electron transparency was determined using the current mode setup and, as mentioned above, a value of 25% was mea-

2014 JINST 9 P02004

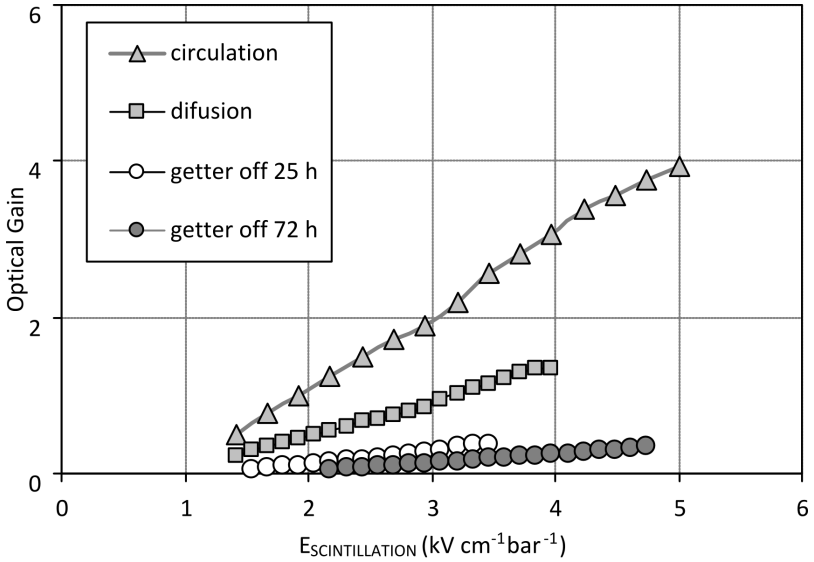

Figure 5. Optical gain in the Zero IBF electron multiplier, for different settings off the purifying getters: solid triangles (getters at 200° C and gas purification by circulation), solid squares (getters at 200°C and gas purification by diffusion only) and solid/open circles (getters off for 72 hours/25 hours). The extraction field at the surface of the photocathode was $0.2\,\mathrm{kV}\times\mathrm{cm}^{-1}\times\mathrm{bar}^{-1}$.

sured when the electric fields in the drift and scintillation regions were set to $60\,\mathrm{V}\times\mathrm{cm}^{-1}\times\mathrm{bar}^{-1}$ as it was the case in the measurements of the signals without the production of the secondary scintillation.

The results obtained for the optical gain are presented in figure 5 as a function of the electric field in the scintillation region, for different settings of gas purification system. As expected the optical gain follows the same trend as the scintillation production in a uniform electric field gap [17], presenting a linear behaviour with a threshold around $0.8\,\mathrm{kV}\times\mathrm{cm}^{-1}\times\mathrm{bar}^{-1}$

The scintillation output and, thus, the optical gain are strongly dependent on the gas purity conditions, controlled here by the operation of the purifying getters and by the level of gas circulation allowed within the test chamber. Higher values of optical gain were achieved with the getters temperature set at 200°C and with the gas circulating through the purifying system and the chamber (solid triangles in figure 5). For the same electric field in the scintillation region the optical gain decreases if, instead of allowing the gas to circulate through the chamber and getters, one of the entrance valves of the chamber is completely closed, relying only on diffusion for the gas purification (solid squares). The optical gain is further decreased if the getters are completely turned off (open circles) and continuously deteriorates as the time without purification increases (solid circles).

For the present detector geometry we do not expect that the optical gain may increase above 4 at $4.0\,\mathrm{kV}\times\mathrm{cm}^{-1}\times\mathrm{bar}^{-1}$. This is because the G2 optical transparency (83%), the CsI photocathode quantum efficiency (∼25%), the photoelectron extraction efficiency (∼20% [22]), the relative average solid angle (∼35% [23]) and the effective area subtended by the photocathode (77%) will impose such limit to the achievable optical gain.

Another effect we've observed, which results from the different levels of gas purification in the chamber, was the reduction of the maximum voltage difference that could be applied to the GEMs

2014 JINST 9 P02004

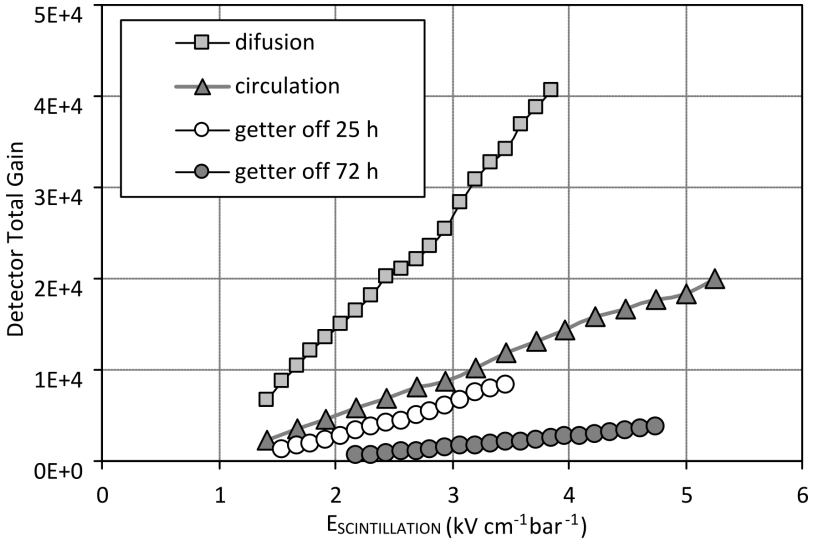

Figure 6. Zero IBF electron multiplier total gain, for different settings of the purifying getters.

of the cascade and, therefore, the reduction of the maximum gain achievable in the GPM, as the gas purity improves. We noticed a reduction on the maximum voltage applied with increasing gas purity. The maximum voltage applicable to the GEM elements of the cascade with the getters at 200°C and with gas circulation was ≈ 420 V (at 1.3 bar), a value significantly lower than the 450 V that could be applied when the gas purification was allowed only by diffusion. This later value is in agreement with past work performed in similar conditions [24]. The maximum voltage difference applicable to the GEM electrodes increased to 490 V, few hours after the getters were turned off. These values were consistently recorded over a period of 800 hours during which the getters were turned on and off for several times. This effect has been investigated in detail in [25], were the maximum gain achieved with a THGEM operating in pure noble gases with different purities have been studied.

4.3 Total gain and energy resolution

The total gain of the Zero IBF electron multiplier is presented in figure 6 as a function of the scintillation field, for different levels of gas purification in the chamber. The total gain depends on both the optical gain and the charge multiplication gain in the GPM, which have opposite dependence on the levels of gas purity as we've seen above. Despite that the highest values of optical gain were obtained with the gas circulating through the chamber (figure 5) the highest values of total gain were measured for the condition of gas purification by diffusion (solid squares). The higher charge gains achieved in the GPM when the gas is purified by diffusion (≈30000) compensate for the lower optical gains obtained in such condition. The maximum charge gain measured on the GPM with the gas circulation through the detector was only ≈4600.

The energy resolution achieved with the Zero IBF electron multiplier, figure 7, reaches values below 20%, for the gas circulation case. These values show that the introduction of a first stage of proportional scintillation production, combined with a CsI photocathode for scintillation readout, does not degrade the energy resolution and overall response of the electron multiplier, when

2014 JINST 9 P02004

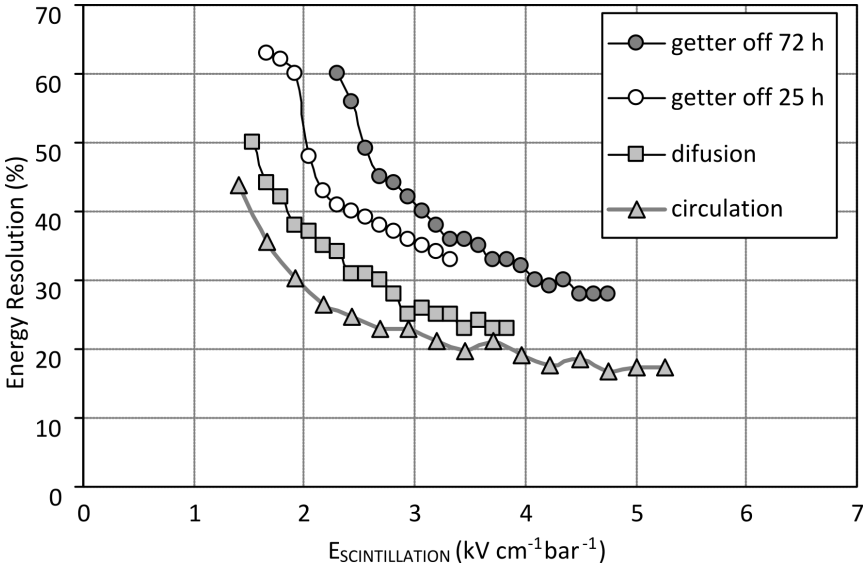

Figure 7. Energy resolution achieved with the Zero IBF electron multiplier.

compared to the one obtained in a conventional electron multiplier based only on charge avalanche amplification [21], in spite of the lower gains achieved in this stage. In addition, optical TPCs in use [26–28] have shown that good 3D event position resolution and pattern readout is also possible to be achieved through the readout of the secondary scintillation.

5 Conclusions

We have presented an electron multiplier having zero IBF and capable to achieve total gain well above 10^4. This Zero IBF electron multiplier has to operate in pure noble gases or their mixtures, xenon in the present case. It has, as a first stage of signal amplification, a proportional secondary scintillation region placed above a CsI photocathode deposited on the top electrode of the first element of a standard cascade multiplier. This multiplier combined with the CsI photocathode act as a GPM for the readout of the proportional secondary scintillation produced in the first stage of the Zero IBF electron multiplier. In the present case, we chose to operate a GPM based on a double-GEM cascade, but any GPM configuration with the desired gain can be used in the zero IBF electron multiplier.

The optical gain achieved in the proportional scintillation region, in terms of the number of photoelectrons extracted to the D-GEM cascade, is below 10 and increases with the gas purity, in opposition to the maximum gain that can be achieved in the GPM. These two opposite dependencies compensate and it is possible to achieve overall gains in the region of 2×10^4 to 5×10^4, for the present Zero IBF electron multiplier, in a wide range of gas purification conditions. The optical gain of this electron multiplier reaches values above 3, with proper gas purity conditions and with an electric field in the scintillation region above $4\,\mathrm{kV}\times\mathrm{cm}^{-1}\times\mathrm{bar}^{-1}$ for xenon. The optical gain of the Zero IBF electron multiplier can be increased by increasing the proportional scintillation gap thickness, the gas pressure and/or the effective area of the CsI photocathode. The relatively modest values of optical gain achieved with the current setup do not compromise the energy resolution of

2014 JINST 9 P02004

the Zero IBF electron multiplier, allowing to obtain better energy resolution that the achieved in a D-GEM cascade in pure xenon [21]. In addition, the overall gain can be increased by adding and/or choosing other electron multiplier elements for the GPM Cascade (GEMs, THGEMs, MHSPs [29] or Micromegas), without destroying the total IBF suppression capability of the proposed device. Therefore, if necessary, it is possible to produce electron multipliers presenting zero IBF with gains as high as 10^6.

Other noble gases such as argon and krypton or mixtures of noble gases may be considered as filling gas for the Zero IBF detector and will be studied in the near future.

Acknowledgments

This work is funded by FEDER, through the Programa Operacional Factores de Competitividade-COMPETE and by National funds through FCT- Fundação para a Ciência e Tecnologia in the frame of project CERN/FP/123614/2011. Fernando D. Amaro was supported by FCT under Post-Doctoral Grant SFRH/BPD/74775/2010.

References

[1] A. Breskin et al., *Ion-induced effects in GEM & GEM/MHSP gaseous photomultipliers for the UV and the visible spectral range*, *Nucl. Instrum. Meth.* **A 553** (2005) 46.

[2] F. Sauli, L. Ropelewski and P. Everaerts, *Ion Feedback Suppression in Time Projection Chambers*, *Nucl. Instrum. Meth.* **A 560** (2006) 269.

[3] A. Bondar, A. Buzulutskov, L. Shekhtman and A. Vasiljev Budker, *Study of ion feedback in multi-GEM structures*, *Nucl. Instrum. Meth.* **A 496** (2003) 325.

[4] J.F.C.A. Veloso et al., *MHSP in reversed-bias operation mode for ion blocking in gas-avalanche multipliers*, *Nucl. Instrum. Meth.* **A 548** (2005) 375.

[5] J.F.C.A. Veloso, F.D. Amaro, J.M.F. dos Santos, A. Breskin, A. Lyashenko and R. Chechik, *The Photon-Assisted Cascaded Electron Multiplier: a concept for potential avalanche-ion blocking*, 2009 *JINST* **1** P08003.

[6] Lyashenko, A. Breskin, R. Chechik, F.D. Amaro, J.F.C.A. Veloso and J.M.F. Dos Santos, *High-gain DC-mode operated Gaseous Photomultipliers for the visible spectral range*, *Nucl. Instrum. Meth.* **A 610** (2009) 161.

[7] F. Sauli, *GEM: a new concept for electron amplification in gas detectors*, *Nucl. Instrum. Meth.* **A 386** (1997) 531.

[8] M. Killenberg et al., *Charge transfer and charge broadening of GEM structures in high magnetic fields*, *Nucl. Instrum. Meth.* **A 530** (2004) 251.

[9] J.F.C.A. Veloso, J.M.F. dos Santos and C.A.N. Conde, *A proposed new microstructure for gas radiation detectors: the microhole and strip plate*, *Rev. Sci. Instrum.* **71** (2000) 2371.

[10] J.M. Maia, J.F.C.A. Veloso, J.M.F. dos Santos, A. Breskin, R. Chechik and D. Mörmann, *Advances in the Micro-Hole & Strip Plate gaseous detector*, *Nucl. Instrum. Meth.* **A 504** (2003) 364.

[11] A.V. Lyashenko, A. Breskin, R. Chechik, J.F.C.A. Veloso, J.M.F. Dos Santos and F.D. Amaro, *Development of high-gain gaseous photomultipliers for the visible spectral range*, 2009 *JINST* **4** P07005.

2014 JINST 9 P02004

[12] F.D. Amaro, J.F.C.A. Veloso, J.M.F. Dos Santos, A. Breskin, R. Chechik and A.V. Lyashenko, *The Photon-Assisted Cascaded Electron Multiplier operation in CF(4) for ion backflow suppression*, *IEEE T. Nucl. Sci.* **55** (2008) 1652.

[13] D. Mormann, A. Breskin, R. Chechik and D. Bloch, *Evaluation and reduction of ion back-flow in multi-GEM detectors*, *Nucl. Instrum. Meth.* **A 516** (2004) 315.

[14] ILD concept group, *International large detector letter of intent*, February 2010.

[15] LCTPC collaboration, *TPC R&D for a Linear Collider Detector*, status report, April 2008.

[16] A. Bagulya et al., *Dynamic distortions in the HARP TPC: observations, measurements, modelling and corrections*, 2009 *JINST* **4** P11014.

[17] J.M.F. dos Santos et al., *Development of portable gas proportional scintillation counters for x-ray spectrometry*, *X-Ray Spectrom.* **30** (2001) 373.

[18] D. Mörmann, A. Breskin, R. Chechik, P. Cwetanski and B.K. Singh, *A gas avalanche photomultiplier with a CsI-coated GEM*, *Nucl. Instrum. Meth.* **A 478** (2002) 230.

[19] C.M.B. Monteiro et al., *Secondary scintillation yield in pure xenon*, 2007 *JINST* **2** P05001.

[20] C.M.B. Monteiro, J.A.M. Lopes, J.F.C.A. Veloso and J.M.F. dos Santos, *Secondary scintillation yield in pure argon*, *Phys. Let.* **B 668** (2008) 167.

[21] T.L. van Vuure, F.D. van den Berg, C.W.E. van Eijk and R.W. Hollander, *Properties of the GEM, double GEM and GEM plus MGC combination*, *Nucl. Instrum. Meth.* **A 443** (2000) 375.

[22] L.C.C. Coelho et al., *Measurement of the photoelectron-collection efficiency in noble gases and methane*, *Nucl. Instrum. Meth.* **A 581** (2007) 190.

[23] J.M.F. dos Santos, A.C.S.S.M. Bento and C.A.N. Conde, *The dependence of the energy resolution of gas proportional scintillation counters on the scintillation region to photomultiplier distance*, *IEEE T. Nucl. Sci.* **39** (1992) 541.

[24] F.D. Amaro et a;., *Operation of a single-GEM in noble gases at high pressures*, *Nucl. Instrum. Meth.* **A 579** (2007) 62.

[25] J. Miyamoto, A. Breskin and V. Peskov, *Gain limits of a Thick GEM in high-purity Ne, Ar and Xe*, 2010 *JINST* **5** P05008.

[26] E. Aprile, XENON100 Collaboration, *The XENON100 dark matter experiment*, *Astropart. Phys.* **35** (2012) 573.

[27] D. Lorca, J. Martín-Albo, F. Monrabal, et al., *The NEXT experiment: a high pressure xenon gas TPC for neutrinoless double beta decay searches*, *Nucl. Instrum. Meth.* **A 718** (2013) 387.

[28] D.Yu. Akimov et al., *The ZEPLIN-III dark matter detector: instrument design, manufacture and commissioning*, *Astropart. Phys.* **27** (2007) 46.

[29] E.D.C. Freitas et al., *Micro-hole and strip plate-based photosensor*, *Nucl. Instrum. Meth.* **A 580** (2007) 214.

2014 JINST 9 P02004